Precise timing of MIS 7 sub-stages from the Austrian Alps

Kathleen A. Wendt[a], Xianglei Li[b], R. Lawrence Edwards[b], Hai Cheng[b,c], Christoph Spötl[a]

[a]Institute of Geology, University of Innsbruck, Innrain 52, 6020 Innsbruck, Austria

5   [b]Department of Earth Sciences, University of Minnesota, 116 Church Street SE, Minneapolis 55455, USA

[c]Institute of Global Environmental Change, Xi'an Jiaotong University, Xi'an 710049, China

Correspondence to: kathleen.wendt@uibk.ac.at

Abstract. Determining the precise timing of glacial terminations and the interglacials that follow is key to addressing questions surrounding future warming. Here, we present a high-precision record of Termination III (TIII), Termination IIIa (TIIIa), the

10 penultimate interglacial (MIS 7), and the penultimate glacial inception (MIS 7/6 transition) from Spannagel Cave in the Austrian Alps. Using state-of-the-art mass spectrometry techniques, we have constructed a uranium-series dated chronology with relative age uncertainties averaging 1.7‰ (2σ) during our study period (247 to 191 thousand years before present). Results reveal the onset of TIII at 242.5±0.2 ka and the duration of MIS 7e between 241.8 to 236.7 (±0.6) ka. Depleted $\delta^{18}O$ values indicating MIS 7b center at 229.5±2.3 ka. An abrupt shift towards higher $\delta^{18}O$ values at 217.1±0.5 ka marks the beginning of

15 TIIIa. Two periods of high $\delta^{18}O$ values (greater than -10‰) between 215.9–213.3 and 204.3–197.5 (±0.4) ka coincide with interglacial substages MIS 7c and 7a, respectively. Two newly collected stalagmites from Spannagel Cave (SPA146 & 183) provide high-resolution replications of the latter portion of the MIS 7a/6e transition, which occurred between approximately 197.1 and 191.4 (±0.3) ka. The resulting multi-stalagmite timeseries provides important chronological constraints on climate shifts in Europe and the North Atlantic during MIS 7. This study also provides a clear answer to the exact timing of TIIIa,

20 which has been previously debated.

1 Introduction

Investigation into past glacial-interglacial cycles and their abrupt transitions provides key insight into the mechanisms that drive climate change. Marine Isotope Stage (MIS) 7 (ca. 246-186 thousand years before present [ka], where present is "1950"

25 CE) stands distinctively apart from the last eight interglacial cycles. Following Termination III (TIII), MIS 7 is comprised of three warm (7e, c, a) and two cold (7d, b) sub-stages, as well as a second glacial termination (TIIIa). MIS 7 has gained increased attention in recent years, as each sub-stage represents an individual case study for the response of the ocean-atmosphere system to varying degrees of external and internal forcings.

30 Determining the precise timing of MIS 7 sub-stages is key in unraveling the mechanisms behind this interesting period in earth's climate history. Yet, obtaining climate records for MIS 7 with sufficient resolution and chronological precision to make

meaningful comparisons has proved challenging. For example, lacustrine and marine records indicate rapid vegetation changes throughout MIS 7 (e.g. Tzedakis et al. 2004; Despart et al. 2006; Roucoux et al. 2008), yet the chronologies of these records are largely dependent on indirect orbital tuning or aligning to benthic $\delta^{18}O$ records. This is a problem, as chronologies of

35   marine benthic $\delta^{18}O$ records often feature uncertainties of ±10 ka during MIS 7 (e.g. LR04 stack; Lisiecki and Raymo 2005). Furthermore, the limited number of independent chronologies that span MIS 7 hinders the ability to intercompare the timing of global changes, including identifying leads, lags and synchronicities across different climate zones.

Here, we turn to speleothems from the Austrian Alps (Fig. 1). The climate of this high alpine region is strongly influenced by

40   atmospheric processes over the North Atlantic Ocean and its sea ice system. Striking similarities between alpine speleothem $\delta^{18}O$ and Greenland ice $\delta^{18}O$ (Spötl and Mangini 2002; Spötl et al. 2006) and North Atlantic marine records (Mangini et al. 2005, 2007) have been observed on centennial to orbital timescales. In particular, speleothem records from the last two interglacial periods indicate a tight coupling between temperatures in the central Alps of Austria to atmospheric circulation over the North Atlantic (Mangini et al. 2007; Meyer et al. 2008). In this study, we aim to determine the precise timing of TIII,

45   TIIIa, and the five sub-stages of MIS 7 recorded in Spannagel Cave located 2500 m above sea level (a.s.l.) in the central Alps of western Austria. Pioneering work by Holzkämper et al. (2005) and Spötl et al. (2007, 2008) presented multiple stalagmites and flowstones deposited throughout MIS 7. Since this study, new developments in high precision isotopic measurement methods by Cheng et al. (2013) and Craig et al. (2016, 2017) allow for ultra-high age precision, with 2σ absolute age uncertainties averaging ±300 years during MIS 7. In addition, two newly discovered stalagmites from Spannagel Cave provide

50   further insight into the penultimate glacial inception (MIS 7/6 transition). The resulting $\delta^{18}O$ record provides a high-precision chronology of abrupt climate change in the European Alps during MIS 7, while addressing the need for absolute-dated terrestrial paleorecords from regions that are sensitive to the North Atlantic realm.

2 Regional setting

The Alps are a climatically sensitive region located in central Europe. Over the last century, the amplitude of change in regional

55   temperatures was twice the mean of the Northern Hemisphere (Auer et al. 2007), contributing to a 26% reduction in Alpine glacier mass over the last few decades (Fischer et al. 2015). The central Alps are situated in the path of the Westerlies and northerly flowing Mediterranean air masses. Back-trajectory studies show that modern precipitation is largely sourced from North Atlantic and Arctic Oceans (63%) and the Mediterranean Sea (21%) (Sodemann and Zubler 2010). Seasonally, the North Atlantic Ocean contributes the majority of moisture during winter and summer, while autumn moisture sources are split

60   between the North Atlantic Ocean and Mediterranean Sea (Sodemann and Zubler 2010). For a given altitude, the $\delta^{18}O$ of rainfall sourced from the North Atlantic Ocean will be depleted relative to Mediterranean sources, due to (i) more depleted isotopic composition of ocean waters and (ii) a longer transport pathway and successive rainout (Kaiser et al. 2002).

Spannagel Cave (Fig. 1; 47°04'54"N 11°40'2"E; 2300 to 2530 m a.s.l.) is located above the timberline in the vicinity of a
65   retreating glacier (Hintertux Glacier) close to the main Alpine crest. Previous publications provide great detail on the setting
of this cave (Spötl et al. 2004; Spötl and Mangini 2007, 2010). A few salient features relevant for this study are summarized
here. Spannagel cave developed in a ca. 20 m-thick Upper Jurassic marble (Hochstegen Formation) sandwiched between gneiss
bedrock. It is a well-ventilated cave system with stable air temperatures in the interior of the cave falling within a narrow range
of +1.8 to +2.2°C (measured at several sites using data loggers over a period of about 20 years). These values are higher by
70   about 2°C than the mean annual air temperature at the elevation of the cave, which is a reflection of the small positive thermal
anomaly due to the ascending geometry of the cave (chimney effect; Spötl and Pavuza 2016). Relative humidity in the cave
interior reaches invariably higher than 96%. Today, the actively retreating Hintertux Glacier terminates ca. 500 m south of
Spannagel cave. During the last glacial maximum, the cave was completed covered by as much as 150-250 m of glacial ice
(van Husen, 1987). The presence of speleothems that grew during several cold climate periods suggests that the Hintertux
75   Glacier has remained largely temperate, or warm-based, in the past (Spötl and Mangini 2007). Under glacial conditions, it is
hypothesized that the oxidation of pyrite in the host rock allowed karst dissolution to proceed in the rock beneath the glacier
without the input of soil-derived carbon dioxide (Spötl and Mangini 2007).

Snowpack melt is the dominate source of recharge to this region and the largest supplier to Spannagel drip waters (Mangini et
80   al. 2005). The $\delta^{18}O$ of modern and late Holocene calcite has been shown to reflect local winter temperatures (Mangini et al.
2005). Other factors influencing Spannagel $\delta^{18}O$ may include: (i) changes in moisture sources and dominant trajectories and
(ii) changes in the seasonal proportions of annual totals (Spötl and Mangini 2007; Spötl et al. 2008). An interesting feature of
Spannagel cave drips waters is that they are rich in U. Cave water range from 5 ppb (small stream in the central cave system)
to 33 ppb (stalactite drip water). As a result, speleothems from this cave are exceptionally high in U concentrations (3 to 399
85   ppm). U is most likely sourced from the overlying gneiss which yielded significantly higher U concentrations (3.4-12.0 ppm)
than the marble (0.3-2.2 ppm).

Stalagmite SPA121 (Fig. S1) was found in the northern segment of the cave embedded in unconsolidated silty sand which
were most likely transported into the cave by high-discharge streams during the last deglaciation. The stalagmite is 19.3 cm
90   tall and was found attached to a platy and angular piece of calcite-cemented gravel. The surface of the sample is covered by a
thin layer of medium gray, clay-rich calcite, but the interior preserves mostly transparent, inclusion-poor calcite, showing a
striking pattern of cracks. The origin of these cracks is enigmatic but may be related to freezing of the cave or the sediments
in which the sample was embedded during cold periods. SPA183 is a 39 cm tall stalagmite collected from the central part of
the cave and a slightly higher altitude than SPA 121. SPA183 revealed three distinct growth axes that are marked by variations
95   in color (Fig. S1). SPA146 is a 24 cm tall stalagmite which grew in the same small chamber as SPA183. It shows two distinct
growth axes (Fig. S1).

3 Methods

Stalagmites SPA121, 146, and 183 were halved and polished. Subsamples for U-Th dates (n=40) were hand drilled along the growth axis of halved stalagmites. Subsample trenches were drilled no larger than 1 mm in width, such that the sampling error (~175 years) remained within the analytical uncertainties (see results). Target sample weights ranged from 200 to 20 mg in concordance with changes in U concentration. Subsamples were spiked with a mixed ^{233}U-^{236}U-^{229}Th spike similar to that described in Edwards et al. (1987). Procedures for U and Th chemical separation and preparation of reagent solutions follow the methods described in Edwards et al. (1987) and Shen et al. (2002).

U and Th isotopic measurements were made on a Thermo Scientific Neptune Plus MC-ICP-MS following the instrument calibration and the Faraday cup measurement method described in Cheng et al. (2013). In addition, a 10^{13} Ohm amplifier was installed within the detection system in order to collect low ion beam intensities (e.g. ^{234}U and ^{230}Th) (Craig et al. 2016, 2017 and references therein). The methods of gain calibration and dynamic time correction of the high resistor are largely based on Craig et al. (2016) and (2017). Each sample was measured for 300s or longer. Intensities of ^{234}U and ^{230}Th beams were on average 15 and 5 mV, respectively.

Stable isotope samples were micromilled continuously along the extension axis of each stalagmite at 0.15-0.20 mm increments. 946 stable isotope measurements on stalagmite SPA121 were previously published in Spötl et al. (2008). 890 and 583 new stable isotope measurements from stalagmites SPA183 and SPA146, respectively, are reported here. Calcite powders were analyzed using a Gasbench II linked to a Delta V Plus isotope ratio mass spectrometer. Values are reported relative to VPDB and the 1-sigma precision is 0.06 and 0.08 ‰ for δ^{13}C and δ^{18}O, respectively.

4 Results

Resulting U-Th ages and their respective replicates are in stratigraphic order within uncertainties (supplementary table 1). This study focuses on the MIS 7 portion of stalagmite SPA121, which was deposited without interruption between 248.5 and 191.5 (±1) ka (see Spötl et al. 2008 for details on all SPA121 growth phases). New U-Th ages for this stalagmite fall within age uncertainties of the previously published ages (Spötl et al. 2008; Fig. 2). Similar δ^{234}U$_i$ values and ^{232}Th and ^{238}U concentrations further underscore a high degree of reproducibility between the two SPA121 data sets. Remarkably, new SPA121 ages improve the precision of previously published age uncertainties by an order of magnitude (Fig. 2), from an average of 1.7% to 0.17%.

The late MIS 7 growth phase of stalagmites SPA183 and SPA146 (Fig. S1) occurred between 191.9-190.6 (±0.6) ka and 191.6-182.3 ±0.3 ka, respectively. The exact onset of growth is unknown, as both stalagmites show evidence of diagenesis spanning first 2-3 cm of the late MIS 7 growth phase (Fig. S2; Table S1). Evidence of diagenetic alteration includes a conspicuously white, milky calcite fabric and U-Th ages that are out of stratigraphic order and unable to be replicated. As a result, this study

focuses only on the unaltered portion of the late MIS 7 growth phases of stalagmites SPA183 and SPA146. Age uncertainties
130   of SPA146 and 183 average 0.09% and 0.16%, respectively. Significantly higher $\delta^{234}U_i$ values from SPA146 and 183 relative
to SPA121 suggest differing drip sources between the first two neighboring stalagmites and SPA121. Growth rates calculated
from new SPA121 ages closely agree with previously published data in Spötl et al. (2008) (Fig. 2). The average growth rate is
5.6 μm/yr, excluding one period of exceptionally low growth rate (0.8 μm/yr) between 231.1 and 219.6 ±0.6 ka. In contrast,
average growth rates of SPA183 and SPA146 are higher (63 and 140 μm/yr, respectively). Differences in growth rates are
135   likely due to differing drip sources.

SPA121 stable isotope values used in this study are from Spötl et al. (2008). New stable isotope data from SPA146 and 183 is
reported in table S2. The range of SPA121 $\delta^{18}O$ values (-8.1 to -14.7‰) and $\delta^{13}C$ values (9.7 to 0.8‰) is in agreement with
newly measured $\delta^{18}O$ values from SPA146 and SPA183 (Fig. 3). Results from Hendy tests on stalagmite SPA121 suggest that
calcite was deposited close to isotopic equilibrium (Spötl et al. 2008). Hendy tests on the new stalagmites SPA146 (averaged
140   R^2=0.88) and SPA183 (averaged R^2=0.84) indicate possible kinetic influences (see Fig. S3), although the replication in the
general trend and absolute values of all three stalagmites argue against significant kinetic effects.

The $\delta^{18}O$ signature of all three stalagmites is depleted relative to modern and Holocene speleothems from this cave, suggesting
145   cooler winter temperatures at the time of deposition. Other possible factors contributing to decreased $\delta^{18}O$ include a greater
portion of North Atlantic Ocean sourced rainfall, either in total amount or due to seasonal changes. The $\delta^{13}C$ signature of all
three stalagmites are higher relative to modern and Holocene speleothems (-10 to -7‰), reflecting a signal that is buffered by
the isotopic composition of the host rock (Spötl et al. 2004). Enriched $\delta^{13}C$ values indicate no significant input of soil C into
the system, thereby indicating an absence of soil and vegetation above the cave throughout the duration of deposition (Spötl
150   et al. 2008). Cooler surface temperatures and the absence of soil argue for a significantly larger Hintertux Glacier during MIS
7 relative to today, likely covering a large portion of the cave. The growth of speleothems during cold climate periods of MIS
7 is likely due to the warm-based nature of Hintertux, allowing the supply of melt water while preventing the cave from
freezing.

155   **5 Discussion**

The new Spannagel $\delta^{18}O$ record spans the entirety of MIS 7 and includes 5 distinct sub-stages, TIII and TIIIa, and the MIS 7/6
glacial inception (table 1). Due to our unprecedented age control, we can determine precise timing and duration of each MIS
7 sub-stage and glacial termination as recorded in the central Alps (Fig. 4; table 1). Following the start of speleothem growth
at 247.3±0.2 ka, an abrupt shift towards higher $\delta^{18}O$ values at 242.5±0.3 ka marks the start of the TIII deglaciation. The ensuing
160   interglacial period (MIS 7e) is characterized by high $\delta^{18}O$ values (greater than -10‰) and spanned 5.5 thousand years (ky)
from 241.8 to 236.0 (±0.3) ka. Depleted $\delta^{18}O$ values (less than -12‰) between 234.3 and 216.9 (±0.3) ka mark MIS 7d, with

maximum cool conditions between 231.3–228.6 (±0.2) ka. An abrupt shift towards higher $\delta^{18}O$ values at 216.8±0.3 ka marks the beginning of TIIIa. Two periods of high $\delta^{18}O$ values between 215.7–212.9 (±0.4) ka (>-10‰) and 201.8–197.1 (±0.5) ka (-8.7‰) coincide with interglacial periods MIS 7c and 7a, respectively. A final shift towards lower $\delta^{18}O$ values from 197.1 to

165   191.4 (±0.3) ka and coincides with the MIS 7/6 transition, the latter portion of which is replicated by stalagmites SPA 146 and 183.

The absolute values of Spannagel $\delta^{18}O$ are lower during MIS 7 warm substages (average -9.2‰) relative to the Holocene (average -7.8‰; Spötl et al. 2004), suggesting cooler winter temperatures in the central Alps relative to today. This is consistent

170   with globally distributed evidence suggesting that Northern Hemisphere temperatures were cooler during MIS 7 (see PAGES 2016). Supporting evidence includes lower sea levels (Robinson et al. 2002; Thompson and Goldstein 2005; Dutton et al. 2009; Andersen et al. 2010; Murray-Wallace 2002) and lower atmospheric pCO$_2$ (Luethi et al. 2008) relative to the Holocene. Remarkable similarities are observed between Spannagel $\delta^{18}O$ and paleorecords that are sensitive to the North Atlantic climate (Fig. 4). These similarities highlight the rapid climatic link between the central European Alps and North Atlantic realm, as

175   observed in later interglacial periods (Holzkämper et al. 2004; Mangini et al. 2007). Most striking is the covariance of Spannagel $\delta^{18}O$ and Chinese Monsoon $\delta^{18}O$ on sub-orbital timescales, which is explained through the following teleconnections: temperature anomalies in the North Atlantic region influence the intensity of heat transport by northern Hadley circulation, which triggers a latitudinal shift in the ascending branch between Handley cells (known as the Intertropical Convergence Zone or ITCZ). Shifts in the ITCZ, in turn, influence the Chinese Monsoon strength (see Cheng et al. 2016 for

180   details). Thus, both Chinese and central Alpine speleothems respond to common mechanisms of climate forcing. Similarities in the timing of suborbital $\delta^{18}O$ fluctuations recorded in both well-dated records suggest that Spannagel $\delta^{18}O$ is a sensitive and faithful recorder of North Atlantic climate changes throughout MIS 7. Here, we examine each sub-stage, as defined by Spannagel $\delta^{18}O$, in comparison to well-dated paleorecords in order to provide new insights into the timing of North Atlantic climate changes.

185

5.1 Onset of deposition

The onset of speleothem deposition in Spannagel Cave coincides with the end of the S8.2 event (Fig. 5). Similar to Heinrich Events, S8.2 is defined as a period of enhanced ice-rafted detritus (IRD) deposition in North Atlantic sediments (Channell et al. 2012) indicating a large meltwater discharge event. Stadial conditions in the North Atlantic realm triggered the propagation

190   of cool, dry air masses across continental Europe (Pérez-Mejías et al. 2017). We interpret the lack of deposition during and prior to the S8.2 event as a proxy for freezing conditions in Spannagel Cave, thereby preventing speleothem growth. Following the S8.2 event, a resumption of warmer North Atlantic conditions contributed to increased vegetation cover in Spain (248 ±2 ka; Pérez-Mejías et al. 2017), an abrupt strengthening of the Chinese Monsoon (247.6 ±0.9 ka; Cheng et al. 2009), and above-freezing temperatures in the central Alps prompting speleothem growth (247.3±0.2 ka).

195

5.2 Termination III

The abrupt increase of Spannagel δ^{18}O between 242.5 to 241.9 ($\pm$0.3) ka is interpreted as TIII. The ~3‰ increase in Spannagel δ^{18}O reflects warming winter temperatures in the central Alps coupled with a decreased proportion of North Atlantic-sourced precipitation relative to today (Mangini et al. 2005; Spötl et al. 2008) likely due to a weakening of the westerlies in response

200   to abrupt Northern Hemisphere warming.

The shift in Spannagel δ^{18}O coincides with remarkable precision to well-dated records that are sensitive to North Atlantic climate changes, including vegetation productivity in the Iberian Peninsula (241.6–240.7 $\pm$1.6 ka; Pérez-Mejías et al. 2017) and Chinese Monsoon intensity (242.8–241.01 $\pm$0.9 ka; Cheng et al. 2009, 2016). The Spannagel timing of TIII additionally

205   coincides (within uncertainties) with an abrupt warming of North Atlantic sea surface temperatures (SST) (Martrat et al. 2007), North Atlantic benthic δ^{18}O (Martrat et al. 2007), and synthetic Greenland δ^{18}O (Barker et al. 2011). Combined, these globally distributed records point to a rapid warming in the North Atlantic region, resulting in an eastward propagation of heat and weakening of the westerlies. Using our high-precision chronology, we assign the onset of abrupt warming to 242.5 $\pm$0.3 ka.

210   Due to our age precision, we can determine a 7.6$\pm$0.3 ky lag in the onset of warming relative to the rise in 65°N summer insolation associated with TIII (Berger, 1978). The observed lag is similar but greater than the 5.1$\pm$0.9 ky lag in regional warming relative to TII, as recorded in a speleothem from Hölloch on the northern rim of the Alps (Moseley et al. 2015). A possible explanation for a longer lag-time may be the low obliquity forcings during TIII, resulting in lower-than-average insolation during boreal summers which may have delayed warming in the central Alps until near-peak insolation.

215

5.3 MIS 7e

Following the MIS 8 glaciation, a period of high δ^{18}O values (-10‰) occurred between 241.8 and 236.0 ($\pm$0.3) ka. Spannagel δ^{18}O values reach a maximum at 240.5 $\pm$0.3 ka coinciding with peak 65°N summer insolation at 241.0 ka (Berger at al. 1978). Spannagel δ^{18}O began a slow decline starting at 236.0$\pm$0.3 ka, followed by an abrupt drop (-9.9 to -12‰) between 236.0 and

220   234.3 ($\pm$0.3) ka into the MIS 7d cool period. This timing coincides with a steady decline of vegetation productivity in the Iberian Peninsula starting at 238.4 $\pm$2 ka (Pérez-Mejías et al. 2017) and a shift towards drier and cooler conditions between ~237 and 239 ka across southern Europe (Tzedakis et al. 2004). Using our age constraints, we establish the duration of MIS 7e in the central European Alps to between 241.8 and 236.0 ($\pm$0.3) ka.

5.4 MIS 7d

225

MIS 7d is characterized by low δ^{18}O values (<-12‰) from 234.3 to 216.9 ±0.3 ka in our samples. We interpret MIS 7d as a period of colder winter temperatures in the central Alps, although uninterrupted stalagmite deposition indicates that temperatures remained above freezing in this cave likely due to insolation effects of the temperate glacier above (Spötl and Mangini 2007).

230

Within this time period, maximum cooling (<-13‰) occurred between 231.3 and 228.6 ±0.3 ka. This period of maximum cooling coincides with the lowest 65°N summer insolation value (387 W/m^2) over the last 800 ka, centered at 230.0 ka (Berger, 1978). During this time, sea level fell between -18.5 m and -21 m relative to modern levels throughout (Dutton et al. 2009), atmospheric pCO$_2$ dipped below 203 ppmv between 229.6 and 220.9 (±4) ka (Luethi et al. 2008), and modeled Greenland δ^{18}O

235 dropped to near-glacial levels (-42‰) (Barker et al. 2011). Remarkable similarities in the shape and timing of maximum MIS 7d conditions between Chinese Monsoon and Spannagel δ^{18}O provide clear evidence for abrupt cooling of the North Atlantic at this time.

In Europe, δ^{13}C records from the Iberian Peninsula (Pérez-Mejías et al. 2017) and pollen records from Albania (Francke et al.

240 2016) and Greece (Tzedakis et al. 2006) indicate glacial-like conditions during MIS 7d. In the Mediterranean realm, increased aridity recorded by Sardinian speleothems between 225 – 221 (±5) ka (Columbu et al. 2019) and Israeli speleothems at 223 ±4 ka (Bar-Matthews et al. 2003) overlap within age uncertainties of Spannagel-determined MIS 7d (Fig. 6). Overall, the Spannagel record provides new age constraints to the timing and duration of maximum stadial conditions in the North Atlantic associated with MIS 7d.

245

Following the 2.7 kyr time period of maximum cooling, Spannagel δ^{18}O values remain low (<-12‰) until 216.8 ±0.3 ka. Low δ^{18}O values may be attributed to depleted North Atlantic Ocean δ^{18}O during this time (Fig. 4, Martrat et al. 2007), thereby sourcing depleted δ^{18}O rainfall to the central Alps. Evidence for low benthic δ^{18}O, low sea levels (Dutton et al. 2009), and melt water pulses in the Black Sea (Badertscher et al. 2011) between ~230 to 217 ka indicate the presence of continental ice sheets,

250 which may have further influenced atmospheric circulation and temperatures over Europe.

5.5 Termination IIIa

The exact timing of TIIIa has been a topic of ongoing debate. For example, the Chinese monsoon record provides an unclear picture of the onset of TIIIa, which was previously defined at 228±0.8 (Cheng et al. 2009) and, more recently, at 217.1 ±0.9

255 ka (Cheng et al. 2016). We argue that the abrupt increase of Spannagel δ^{18}O between 216.8 and 216.1 (±0.5) ka provides strong evidence for the timing of TIIIa defined in Cheng et al. (2016). The onset of warming in the central Alps also agrees with start

of North Atlantic SSTs warming (217.6 ka), increasing modeled Greenland δ^{18}O (217.4 ka), and high obliquity and precession forcings. The Spannagel-defined onset of TIIIa occurred 1.2 ±0.3 kyr after peak 65°N summer insolation.

260 **5.6 MIS 7c-a**

High δ^{18}O values associated with MIS 7c occur between 215.7 and 212.9 (±0.4) ka, with slightly lower values (~ -10.6‰) extending until 212.0 ±0.4 ka. δ^{18}O drops abruptly between 212.0 and 211.7 (±0.4) ka and remains low between 211.7 and 204.1 (±0.4) ka. This period of depleted δ^{18}O values coincides within uncertainties with low 65°N summer insolation (207 ka) associated with MIS 7b. Spannagel δ^{18}O rises between 204.1 and 201.5 (±0.4) ka and remains high for the remainder of MIS

265 7a until 197.1 (±0.3) ka.

Maximum δ^{18}O values during MIS 7a-c indicate warmer winter temperatures in the central Alps relative to MIS 7e, with MIS 7a the warmest sub-stage. These results support planktonic foraminiferal assemblages on an Iberian Margin sediment core which suggest higher winter temperatures (+1.5°C) during MIS 7a relative to MIS 7e (Desprat et al. 2006). Evidence for a

270 partial retreat of the Hintertux glacier, as suggested by four florescent inclusions or "dust layers" described in detail in Spötl et al. (2008), occurred at 214.3 ±0.4 ka under maximum MIS 7c δ^{18}O. This partial retreat (or repeated partial retreats) of the local glacier points to warmer summer temperatures in the central European Alps at this time.

This generalized pattern of MIS 7 warm periods is also reflected in European pollen data, which indicate that MIS 7c-a had

275 the longest duration, the most diverse and complete forest succession, and the warmest temperatures relative to MIS 7e (Penaud et al. 2008; Tzedakis et al. 2004). Evidence for peak interglacial conditions during MIS 7a is also observed in Mediterranean sapropel deposits (Bar-Matthews et al. 2000; Zanchetta et al. 2007; Ziegler et al. 2010) and prolonged humid conditions in southern Italy (Columbu et al. 2019). Warmer conditions in the central Alps during MIS 7c and 7a relative to MIS 7e may be linked to stronger obliquity and insolation forcings at this time.

280

5.7 MIS 7-6 transition

A drop in Spannagel δ^{18}O starting at 197.1 ±0.2 ka marks the end of MIS 7a in the central Alps. We define the Spannagel MIS 7/6 transition to between 197.1-191.4 (±0.3) ka, with a gradual depletion of δ^{18}O continuing until approximately 187 ka. The defined time period coincides with a drop Mediterranean Sea levels, as shown by Bard et al. (2002).

285

Two newly collected stalagmites from this cave (SPA146 & 183) provide additional records of the late MIS 7a/6e transition and early MIS 6e. The stalagmites grew between 191.8 and 182.3 (±0.6) ka. Similar δ^{18}O values during the overlapping growth

periods highlight the degree of reproducibility between all three records. Lack of stalagmite growth after 182.3 ±0.2 ka suggests

unfavorable conditions in Spannagel Cave, possibly related to due to partly cold-base conditions of the glacier above the cave.

290

6 Conclusions

The limited number of independently dated MIS 7 records hinders an intercomparison of the timing of global climate changes. To address this issue, we present the first ever paleo-record of MIS 7 with relative age uncertainties <2‰. Using this chronology, we can determine the precise timing and duration of MIS 7 sub-stages and associated terminations in the Austrian

295 Alps (table 1). The MIS 7 Spannagel Cave $\delta^{18}O$ record reveals the precise timing and duration of winter temperature changes in the sensitive central Austrian Alps, while providing new insight into temperature and atmospheric circulation changes in the North Atlantic realm. Finally, this study provides critically needed age constraints on the timing of TIIIa.

Author contribution

K.W. and X.L. conducted measurements and analyzed results. H.C., R.L.E., and. C.S. provided scientific guidance, laboratory

300 facilities, and funding. All authors contributed to the final manuscript. Special thanks to M. Wimmer and M. Pythoud for their assistance in the laboratory.

Acknowledgments

This research was partly funded by grants from the Austrian Science Fund (FWF) awarded to C.S.

305 **References**

Andersen, M. B., Stirling, C. H., Potter, E. K., et al.: The timing of sea-level high-stands during Marine Isotope Stages 7.5 and 9: constraints from the uranium-series dating of fossil corals from Henderson Island, Geochimica et Cosmochimica Acta, 74, 3598–3620, doi:10.1016/j.gca.2010.03.020, 2010.

Auer, I., Böhm, R., Jurkovic, A., et al.: HISTALP—historical instrumental climatological surface time series of the Greater 310 Alpine Region, International Journal of Climatology, 27, 17-46, doi:10.1002/joc.1377, 2007.

Badertscher, S., Fleitmann, D., Cheng, H., et al.: Pleistocene water intrusions from the Mediterranean and Caspian seas into the Black Sea, Nature Geoscience, 4, 236-239, doi:10.1038/ngeo1106, 2011.

Bar-Matthews, M., Ayalon, A., Gilmour, M., Matthews, A., and Hawkesworth, C. J.: Sea–land oxygen isotopic relationships from planktonic foraminifera and speleothems in the Eastern Mediterranean region and their implication for paleorainfall 315 during interglacial intervals, Geochimica et Cosmochimica Acta, 67, 3181–3199, doi:10.1016/S0016-7037(02)01031-1, 2003.

Bard, E., Antonioli, F., and Silenzi, S.: Sea-level during the penultimate interglacial period based on a submerged stalagmite from Argentarola Cave (Italy), Earth and Planetary Science Letters, 196, 135–146, doi:10.1016/S0012-821X(01)00600-8, 2002.

320 Barker, S., Knorr, G., Edwards, R. L., et al.: 800,000 years of abrupt climate variability, Science, 334, 347–351, doi:10.1126/science.1203580, 2011.

Berger, A.: Long-term variations of daily insolation and Quaternary climatic changes, Journal of the Atmospheric Sciences, 35, 2362–2367, doi: 10.1175/1520-0469(1978)035<2362:LTVODI>2.0.CO;2, 1978.

Channell, J. E., Hodell, D. A., Romero, O., et al.: A 750-kyr detrital-layer stratigraphy for the North Atlantic (IODP sites
325 U1302–U1303, Orphan Knoll, Labrador Sea), Earth and Planetary Science Letters, 317, 218–230, doi:10.1016/j.epsl.2011.11.029, 2012.

Cheng, H., Edwards, R. L., Shen, C. C., et al.: Improvements in ^{230}Th dating, ^{230}Th and ^{234}U half-life values, and U–Th isotopic measurements by multi-collector inductively coupled plasma mass spectrometry, Earth and Planetary Science Letters, 371, 82–91, doi:10.1016/j.epsl.2013.04.006, 2013.

330 Cheng, H., Edwards, R. L., Broecker, W. S., et al.: Ice age terminations, Science, 326, 248-252, doi: 10.1126/science.1177840, 2009.

Cheng, H., Edwards, R. L., Sinha, A., et al.: The Asian monsoon over the past 640,000 years and ice age terminations, Nature, 534, 640–646, doi:10.1038/nature1859, 2016.

Columbu, A., Spötl, C., De Waele, J., Yu, T. L., Shen, C. C., and Gázquez, F.: A long record of MIS 7 and MIS 5 climate
335 and environment from a western Mediterranean speleothem (SW Sardinia, Italy), Quaternary Science Reviews, 220, 230–243, doi:10.1016/j.quascirev.2019.07.023, 2019.

Craig, G., Hu, Z., Zhang A., Lloyd N. S., Bouman C., and Schwieters J. B.: Dynamic time correction for high precision isotope ratio measurements: Thermo Scientifc Neptune Plus MC-ICP-MS with 10^{13} Ω amplifer technology, Thermo Scientific technical note 30396, 2017.

340 Craig, G., Bouman, C., Lloyd, N., Trinquier, A., Schwieters, J.B.: Dynamic response time correction algorithms for high precision isotope ratio measurements using high gain current amplifier technology Goldschmidt Conf. Abstr. 554, 2016.

Denniston, R. F., Houts, A. N., Asmerom, Y. et al: A stalagmite test of North Atlantic SST and Iberian hydroclimate linkages over the last two glacial cycles, Climate of the Past, 14, doi:10.5194/cp-14-1893-2018, 2018.

Desprat, S., Goñi, M. F. S., Turon, J. L., Duprat, J., Malaizé, B., and Peypouquet, J. P.: Climatic variability of Marine
345 Isotope Stage 7: direct land–sea–ice correlation from a multiproxy analysis of a north-western Iberian margin deep-sea core, Quaternary Science Reviews, 25,1010–1026, doi:10.1016/j.quascirev.2006.01.001, 2006.

Dutton, A., Bard, E., Antonioli, F., Esat, T. M., Lambeck, K., and McCulloch, M. T.: Phasing and amplitude of sea-level and climate change during the penultimate interglacial, Nature Geoscience, 2, 355–359, doi:10.1038/ngeo470, 2009.

Edwards, R. L., Chen, J. H., and Wasserburg, G. J.: ^{238}U-^{234}U-^{230}Th-^{232}Th systematics and the precise measurement of time
350 over the past 500,000 years, Earth and Planetary Science Letters, 81, 175–192, doi:10.1016/0012-821X(87)90154-3, 1987.

Fischer, A., Seiser, B., Stocker Waldhuber, M., Mitterer, C., and Abermann, J.: Tracing glacier changes in Austria from the Little Ice Age to the present using a lidar-based high-resolution glacier inventory in Austria, The Cryosphere, 9, 753–766, doi:10.5194/tc-9-753-2015, 2015.

Francke, A. Wagner, B. Just, J. et al: Sedimentological processes and environmental variability at Lake Ohrid (Macedonia,
355 Albania) between 637 ka and the present, Biogeosciences, 13, 1179–1196, doi: 10.5194/bg-13-1179-2016, 2016.

Holzkämper, S., Spötl, C., and Mangini, A.: High-precision constraints on timing of Alpine warm periods during the middle to late Pleistocene using speleothem growth periods, Earth and Planetary Science Letters, 236, 751–764, doi: 10.1016/j.epsl.2005.06.002, 2005.

Kaiser, A., Scheifinger, H., Kralik, M., Papesch, W., Rank, D., and Stichler, W.: Links between meteorological conditions and spatial/temporal variations in long-term isotope records from the Austrian precipitation network, IAEA-CSP, 13/P., 2002.

Lisiecki, L. E., and Raymo, M. E.: A Pliocene-Pleistocene stack of 57 globally distributed benthic $\delta^{18}O$ records, Paleoceanography, 20, doi:10.1029/2004PA001071, 2005.

Lüthi, D., Le Floch, M., Bereiter, B. et al. (2008). High-resolution carbon dioxide concentration record 650,000–800,000 years before present, Nature, 453, 379–382, doi:10.1038/nature06949, 2008.

Mangini, A., Spötl, C., and Verdes, P.: Reconstruction of temperature in the Central Alps during the past 2000 yr from a $\delta^{18}O$ stalagmite record, Earth and Planetary Science Letters, 235, 741–751, doi:10.1016/j.epsl.2005.05.010, 2005.

Mangini, A., Verdes, P., Spötl, C., Scholz, D., Vollweiler, N., and Kromer, B.: Persistent influence of the North Atlantic hydrography on central European winter temperature during the last 9000 years, Geophysical Research Letters, 34, doi:10.1029/2006GL028600, 2007.

Martrat, B., Grimalt, J. O., Shackleton, N. J., de Abreu, L., Hutterli, M. A., and Stocker, T. F., Four climate cycles of recurring deep and surface water destabilizations on the Iberian margin, Science, 317, 502–507, doi:10.1126/science.1139994, 2007.

Meyer, M. C., Spötl, C., and Mangini, A.: The demise of the Last Interglacial recorded in isotopically dated speleothems from the Alps, Quaternary Science Reviews, 27, 476–496, doi:10.1016/j.quascirev.2007.11.005, 2008.

Moseley, G. E., Spötl, C., Cheng, H., Boch, R., Min, A., and Edwards, R. L.: Termination-II interstadial/stadial climate change recorded in two stalagmites from the north European Alps, Quaternary Science Reviews, 127, 229–239, doi:10.1016/j.quascirev.2015.07.012, 2015.

Murray-Wallace, C. V.: Pleistocene coastal stratigraphy, sea-level highstands and neotectonism of the southern Australian passive continental margin—a review, Journal of Quaternary Science, 17, 469–489, doi: 10.1002/jqs.717, 2002.

Past Interglacials Working Group of PAGES: Interglacials of the last 800,000 years, Reviews of Geophysics, 54, 162–219, doi:10.1002/2015RG000482, 2016.

Penaud, A., Eynaud, F., Turon, J. L., Zaragosi, S., Marret, F., and Bourillet, J. F.: Interglacial variability (MIS 5 and MIS 7) and dinoflagellate cyst assemblages in the Bay of Biscay (North Atlantic), Marine Micropaleontology, 68, 136–155, doi:10.1016/j.marmicro.2008.01.007, 2008.

Pérez-Mejías, C., Moreno, A., Sancho, C. et al: Abrupt climate changes during Termination III in Southern Europe. Proceedings of the National Academy of Sciences, 114, 10047–10052, doi: 0.1073/pnas.1619615114, 2017.

Reille, M., Andrieu, V., de Beaulieu, J. L., Guenet, P., and Goeury, C., A long pollen record from Lac du Bouchet, Massif Central, France: for the period ca. 325 to 100 ka BP (OIS 9c to OIS 5e), Quaternary Science Reviews, 17, 1107–1123, doi:10.1016/S0277-3791(97)00093-0, 1998.

Robinson, L. F., Henderson, G. M., and Slowey, N. C.: U–Th dating of marine isotope stage 7 in Bahamas slope sediments, Earth and Planetary Science Letters, 196, 175–187, doi:10.1016/S0012-821X(01)00610-0, 2002.

Roucoux, K. H., Tzedakis, P. C., Frogley, M. R., Lawson, I. T., and Preece, R. C.: Vegetation history of the marine isotope stage 7 interglacial complex at Ioannina, NW Greece, Quaternary Science Reviews, 27, 1378–1395, doi:10.1016/j.quascirev.2008.04.002, 2008.

Shen, C. C., Edwards, R. L., Cheng, H. et al: Uranium and thorium isotopic and concentration measurements by magnetic sector inductively coupled plasma mass spectrometry, Chemical Geology, 185, 165–178, doi:10.1016/S0009-2541(01)00404-1, 2002.

Sodemann, H. and Zubler, E.: Seasonal and inter-annual variability of the moisture sources for Alpine precipitation during 1995–2002, International Journal of Climatology, 30, 947–961, doi:10.1002/joc.1932, 2010.

Spötl, C. and Mangini, A.: Stalagmite from the Austrian Alps reveals Dansgaard–Oeschger events during isotope stage 3: Implications for the absolute chronology of Greenland ice cores, Earth and Planetary Science Letters, 203, 507–518, doi:10.1016/S0012-821X(02)00837-3, 2002.

405 Spötl, C. and Mangini, A.: Speleothems and paleoglaciers, Earth and Planetary Science Letters, 254, 323–331, doi:10.1016/j.epsl.2006.11.041, 2007.

Spoetl, C. and Mangini, A.: Paleohydrology of high-elevation, glacier-influenced karst system in the central Alps (Austria), Austrian Journal of Earth Sciences, 103, 2010.

Spötl, C., Mangini, A., Bums, S. J., Frank, N., and Pavuza, R.: Speleothems from the high-alpine Spannagel cave, Zillertal Alps (Austria), Studies of cave sediments, 243-256, doi: 10.1007/978-1-4419-9118-8_13, 2004.

410 Spötl, C., Mangini, A., and Richards, D. A.: Chronology and paleoenvironment of Marine Isotope Stage 3 from two high-elevation speleothems, Austrian Alps, Quaternary Science Reviews, 25, 1127–1136, doi:10.1016/j.quascirev.2005.10.006, 2006.

Spötl, C., Scholz, D., and Mangini, A.: A terrestrial U/Th-dated stable isotope record of the Penultimate Interglacial, Earth and Planetary Science Letters, 276, 283–292, doi:10.1016/j.epsl.2008.09.029, 2008.

415 Spötl, C., Holzkämper, S., and Mangini, A.: The Last and the Penultimate Interglacial as recorded by speleothems from a climatically sensitive high-elevation cave site in the Alps, Developments in Quaternary Science Series (Elsevier), 7, 471–491, doi:10.1016/S1571-0866(07)80056-X, 2007.

Spötl, C. and Pavuza, R.: Höhlenatmosphäre, Höhlen und Karst in Österreich, Linz, Oberösterreichisches Landesmuseum, 123–138, ISBN: 978-3854743217, 2016.

420 Thompson, W. G. and Goldstein, S. L.: Open-system coral ages reveal persistent suborbital sea-level cycles, Science, 308, 401–404, doi: 10.1126/science.1104035, 2005.

Tzedakis, P. C., Roucoux, K. H., De Abreu, L., and Shackleton, N. J.: The duration of forest stages in southern Europe and interglacial climate variability, Science, 306, 2231–2235, doi:10.1126/science.1102398, 2004.

van Husen, D.: Die Ostalpen in den Eiszeiten, Geologische Bundesanstalt, Vienna, 1–24, ISBN:3900312583, 1987.

425 Zanchetta, G., Drysdale, R. N., Hellstrom, J. C., Fallick, A. E., Isola, I., Gagan, M. K., and Pareschi, M. T.: Enhanced rainfall in the Western Mediterranean during deposition of sapropel S1: stalagmite evidence from Corchia cave (Central Italy), Quaternary Science Reviews, 26, 279–286, doi: 10.1016/j.quascirev.2006.12.003, 2007.

Ziegler, M., Tuenter, E., and Lourens, L. J.: The precession phase of the boreal summer monsoon as viewed from the eastern Mediterranean (ODP Site 968), Quaternary Science Reviews, 29, 1481–1490, doi:10.1016/j.quascirev.2010.03.011, 2010.

430
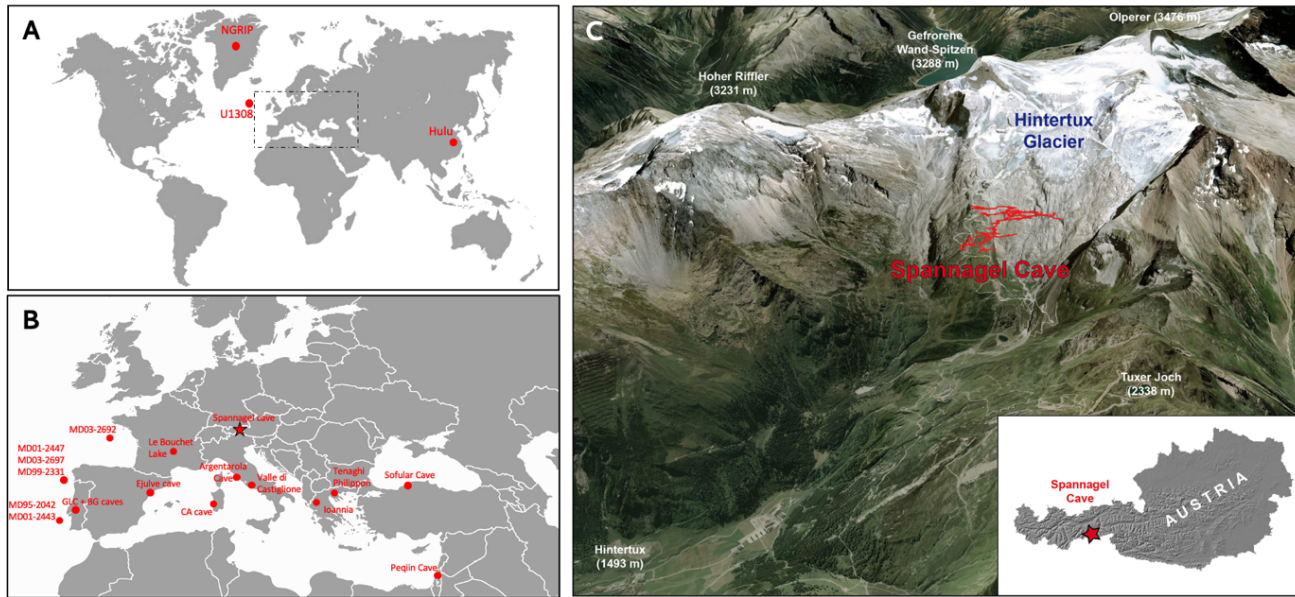
Figure 1: (A) Map indicating the location of paleorecords described in this paper. Black dashed box expanded in (B). (C) Head of the Tux Valley showing the location of Spannagel cave adjacent to the glaciated main ridge of the central Alps (oblique view towards SSE) © Google Earth.

435
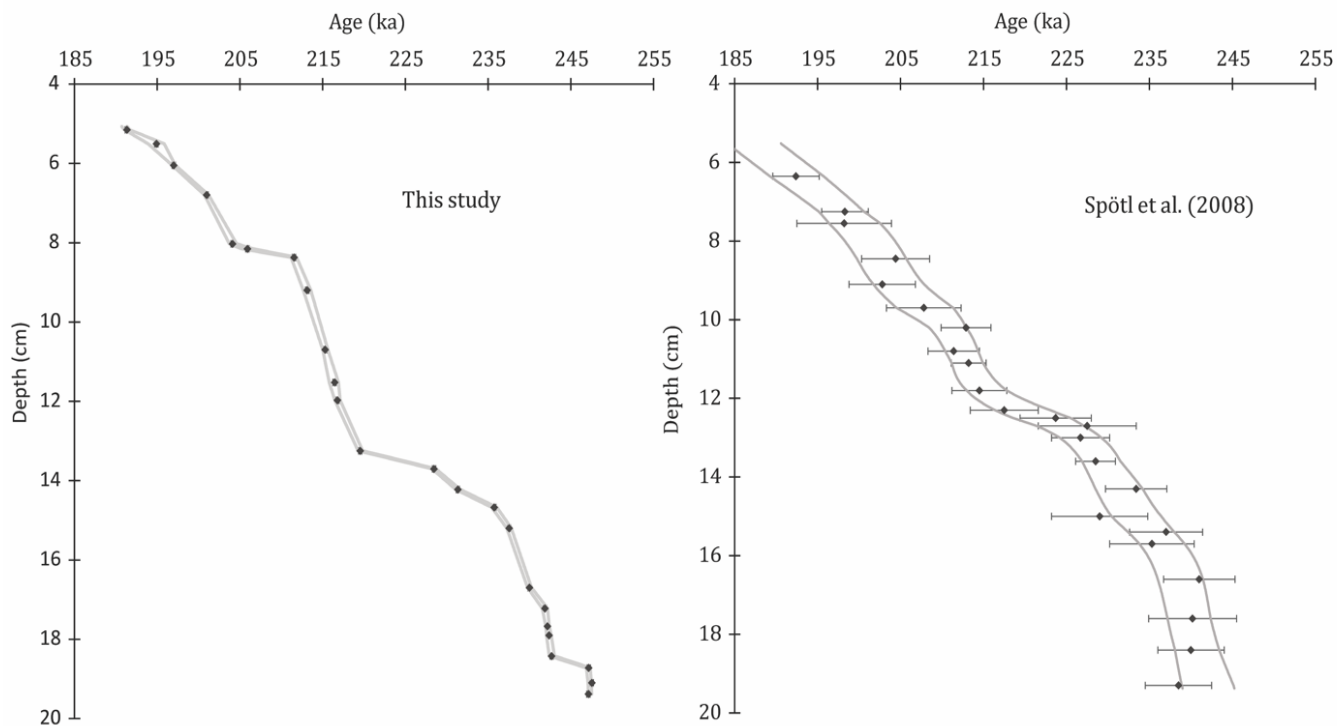
Figure 2: Depth versus age along the growth axis of stalagmite SPA121 with associated 2 sigma age uncertainties from this study (left) and Spötl et al. (2008) (right). Grey lines show upper and lower age model boundaries.

440
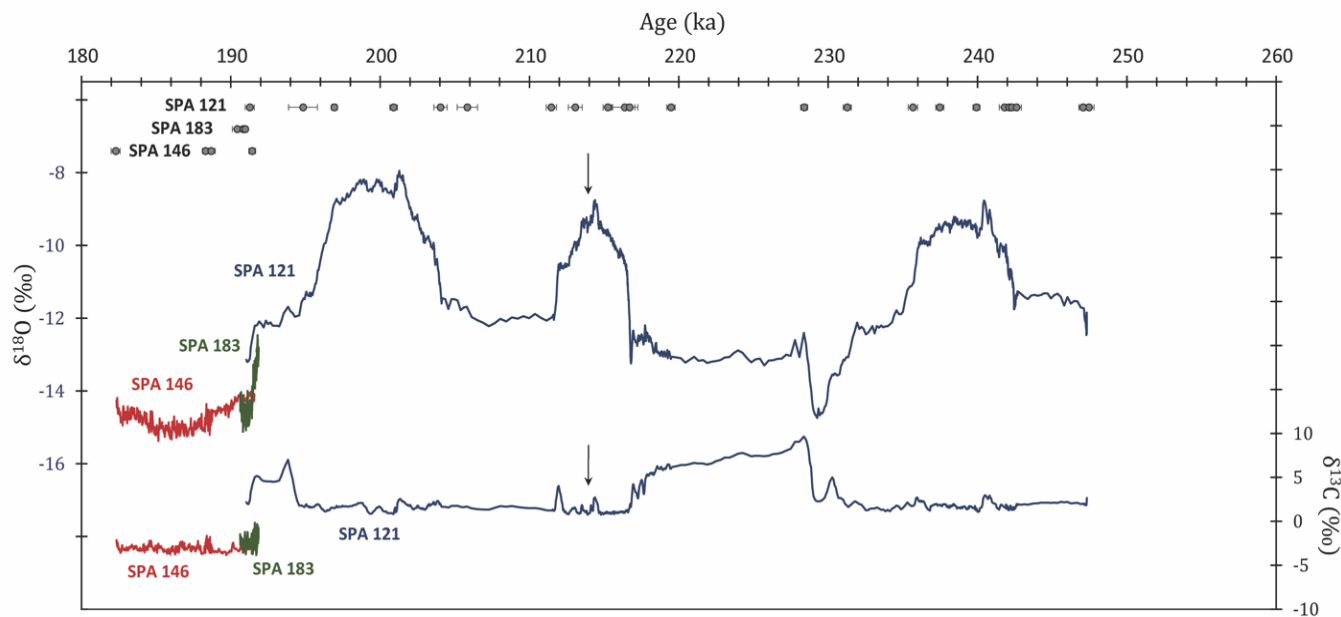
Figure 3: δ¹⁸O and δ¹³C records of stalagmite SPA121 (blue) compared to the shorter growth intervals of stalagmites SPA183 (green) and SPA146 (red). At top, U-Th age results with associated 2 sigma uncertainties. Black arrows indicate location of the dust layer in stalagmite SPA121 (see text).

445

Event	Start (ka)	End (ka)	Duration (ky)
TIII	242.5 ±0.3	241.8 ±0.3	0.7
MIS 7e	241.8 ±0.3	236.0 ±0.3	5.8
MIS 7d	234.3 ±0.3	228.6 ±0.3	5.7
Max MIS 7b cooling	231.3 ±0.3	228.6 ±0.2	2.7
TIIIa	216.8 ±0.3	216.1 ±0.4	0.7
MIS 7c	215.7 ±0.4	212.9 ±0.4	2.8
MIS 7b	211.7 ±0.4	204.1 ±0.4	7.6
MIS 7a	201.8 ±0.3	197.1 ±0.2	4.7
MIS 7/6 transition	197.1 ±0.2	191.4±0.3	5.7

450 **Table 1: The timing and duration of MIS 7 sub-stages and the MIS 7/6 transition, as defined by the Spannagel δ¹⁸O record (see text for detailed definitions).**
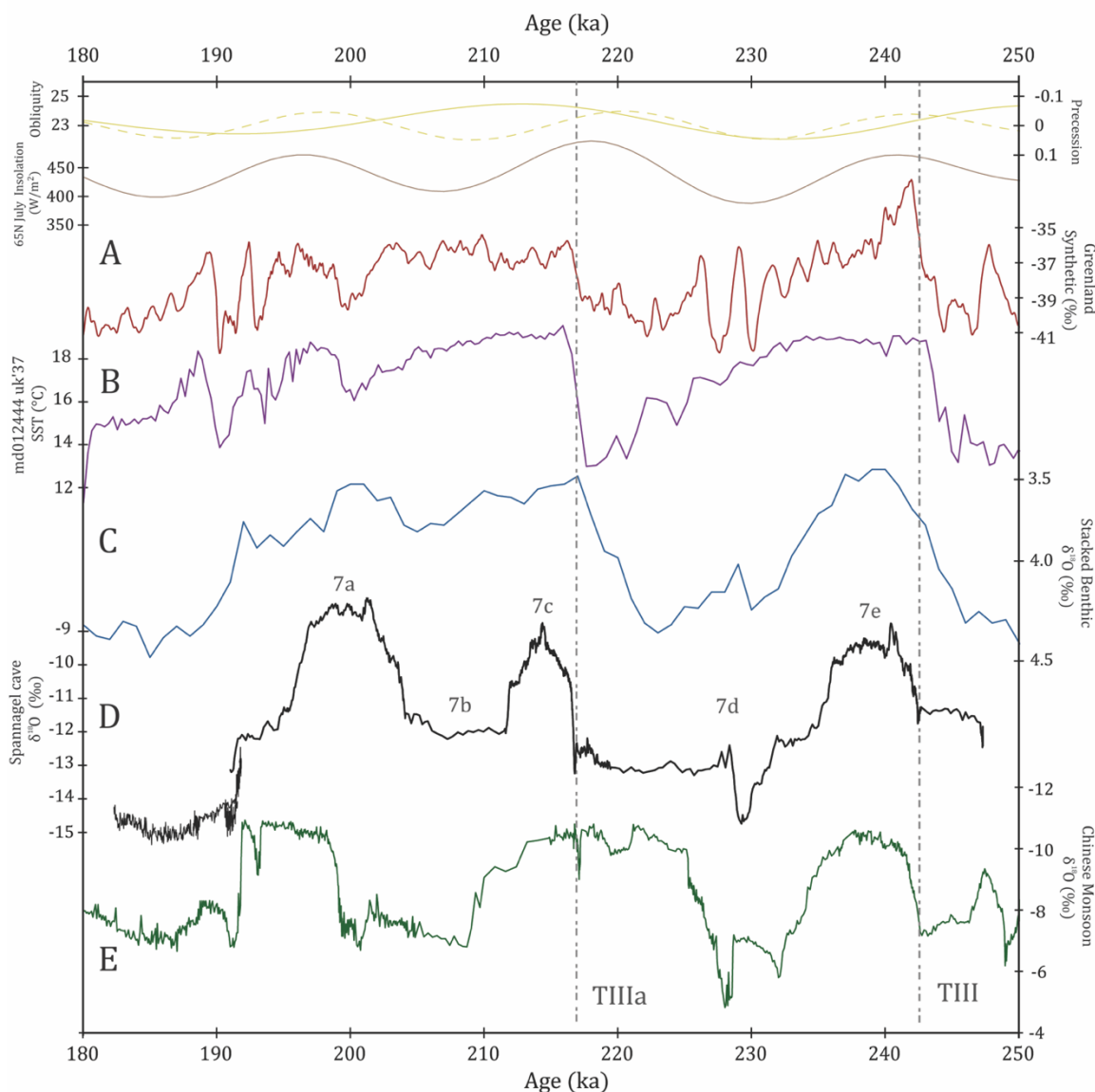
Figure 4: Obliquity (solid yellow), precession (dashed yellow), and 65°N July insolation (brown) from Berger (1978) plotted against (A) Greenland synthetic δ18O (Barker et al. 2011), (B) North Atlantic SST (Martrat et al. 2007), (C) stacked marine benthic δ18O (Lisiecki and Raymo, 2005), (D) Spannagel δ18O from the central Alps (this study), (E) Sanbao cave in eastern China (orange; Cheng et al. 2009, 2016). MIS 7 sub-stages, Terminations III and IIIa, and the MIS 7/6 transition labelled, as defined by the Spannagel δ18O record.
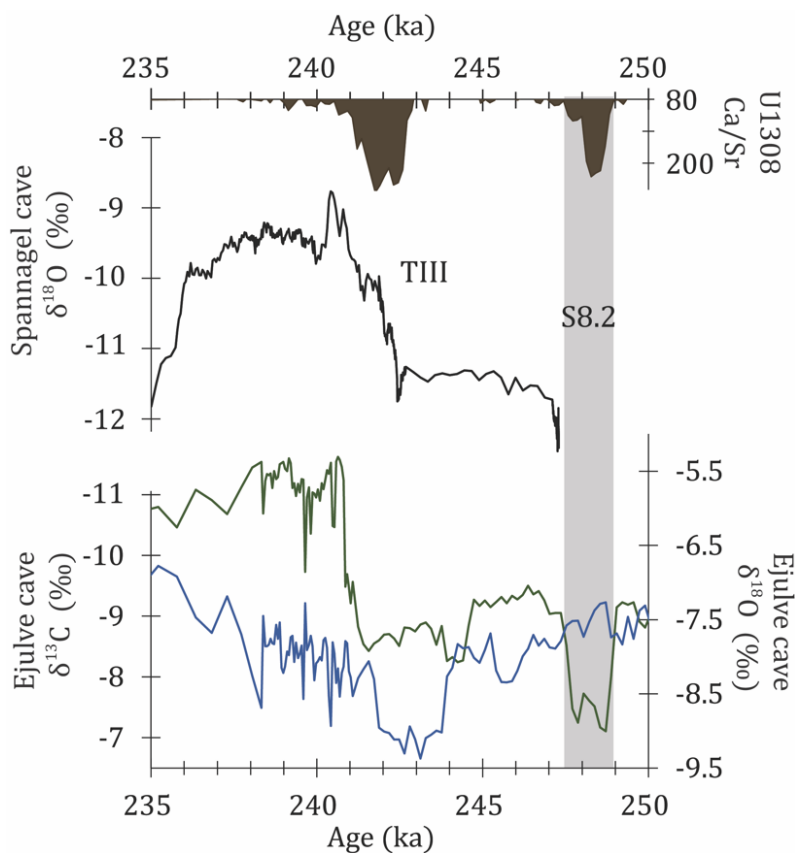
Figure 5: North Atlantic IRD proxy from sediment core U1308 (brown; Channell et al. 2012), Spannagel Cave δ18O from the central Alps (black; this study), and Ejulve cave δ18O (blue) and δ13C (green) from southeastern Spain (Pérez-Mejías et al. 2017). Millennial-scale event S8.2 highlighted in grey.

465
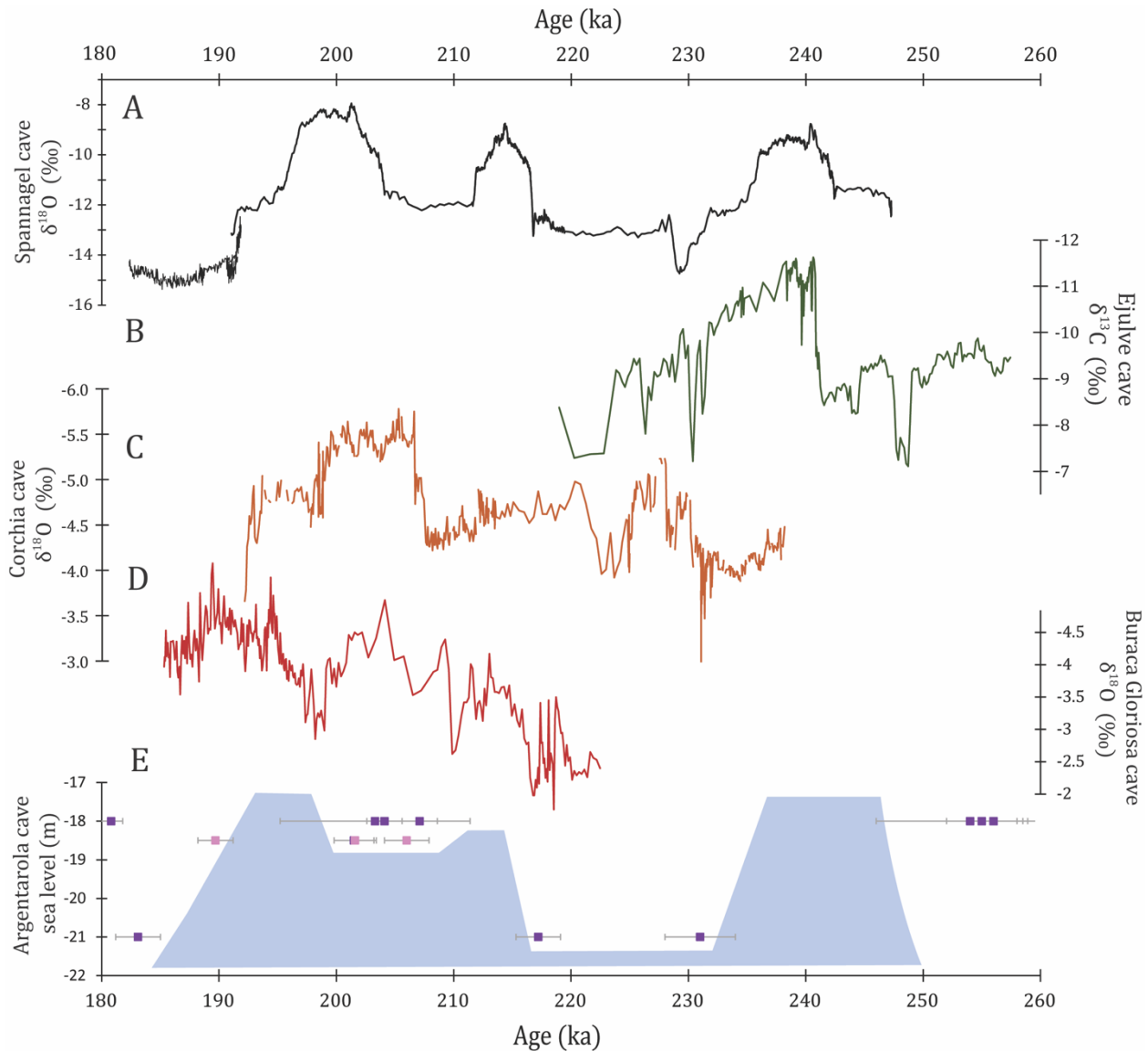
Figure 6: Independently dated MIS 7 records from the circum-Mediterranean region. (A) Spannagel Cave (black; this study), (B) Ejulve cave in southern Spain (green; Pérez-Mejías et al. 2017), (C) Corchia cave in southern Italy (orange; Columbu et al. 2019),
470 **(D) Buraca Gloriosa cave in Portugal (Denniston et al. 2018), (E) Mediterranean Sea-level reconstructions (purple; Dutton et al. 2009) and (pink; Bard et al. 2002); purple shading is for visual aid only as absolute high and low stands are unknown.**